

# I know What You *Sync*: Covert and Side Channel Attacks on File Systems via *syncfs*

Cheng Gu

Department of Computer  
Science and Engineering  
University of California, Riverside  
cgu024@ucr.edu

Yicheng Zhang

Department of Electrical  
and Computer Engineering  
University of California, Riverside  
yzhan846@ucr.edu

Nael Abu-Ghazaleh

Department of Computer  
Science and Engineering  
University of California, Riverside  
nael@cs.ucr.edu

**Abstract**—Operating Systems enforce logical isolation using abstractions such as processes, containers, and isolation technologies to protect a system from malicious or buggy code. In this paper, we show new types of side channels through the file system that break this logical isolation. The file system plays a critical role in the operating system, managing all I/O activities between the application layer and the physical storage device. We observe that the file system implementation is shared, leading to timing leakage when using common I/O system calls. Specifically, we found that modern operating systems take advantage of any flush operation (which saves cached blocks in memory to the SSD or disk) to flush all of the I/O buffers, even those used by other isolation domains. Thus, by measuring the delay of *syncfs*, the attacker can infer the I/O behavior of victim programs. We then demonstrate a *syncfs* covert channel attack on multiple file systems, including both Linux native file systems and the Windows file system, achieving a maximum bandwidth of 5 Kbps with an error rate of 0.15% on Linux and 7.6 Kbps with an error rate of 1.9% on Windows. In addition, we construct three side-channel attacks targeting both Linux and Android devices. On Linux devices, we implement a website fingerprinting attack and a video fingerprinting attack by tracking the write patterns of temporary buffering files. On Android devices, we design an application fingerprinting attack that leaks application write patterns during boot-up. The attacks achieve over 90% F1 score, precision, and recall. Finally, we demonstrate that these attacks can be exploited across containers implementing a container detection technique and a cross-container covert channel attack.

## 1. Introduction

Security and privacy issues in multi-user operating systems (OS) and application software have drawn significant attention from both academia and industry over the past decades. These systems enable concurrent access by multiple users, facilitating efficient sharing of computing resources at both hardware and software levels. At the hardware level, research has identified a series of side-channel attacks targeting shared CPU caches [1], [2], [3], hardware sensors (*e.g.*, accelerometers, camera and gyroscope) [4], [5], [6], DRAM [7], [8], interconnects [9], [10], GPUs [11],

[12], FPGAs [13], [14] and more. On the software side, numerous studies have revealed security vulnerabilities in public OS-provided APIs, leading to OS-level side-channel attacks on systems like iOS [15], [16], Android [17], [18], and Linux [19], [20].

This paper explores OS-level side channels within file systems. File system synchronization is a critical function in the OS, ensuring that data is consistently written from volatile memory (*e.g.*, DRAM) to stable storage (*e.g.*, SSD or disk drive). This process is essential for data integrity, as it guarantees that recent changes are reliably saved, reducing data loss in the event of a system crash or power failure. Synchronization mechanisms are also integral to many OS optimizations, which improve system performance and resilience. To boost performance, techniques such as batching, scheduling, buffering, and caching are widely implemented [21], [22], [23], [24]. To enhance durability against potential failures, mechanisms such as journaling, write-ahead logging, and copy-on-write are employed [25], [26], [27], [28].

As storage device capacities continue to increase into 10s of terabytes or more, it is increasingly common for multiple programs to share the same disk, whether on local machines or cloud-based servers [29], [30], [31]. File system synchronization methods like *syncfs* play a crucial role in efficiently and reliably managing data in such shared environments. Unlike the more granular *fsync*, which flushes changes for individual files, *syncfs* operates at the file system level, flushing all pending changes across multiple files in a single call. This approach simplifies synchronization and enhances performance by reducing the overhead associated with multiple *fsync* calls. While these optimizations enhance performance and durability, they also create new avenues for information leakage.

Recent work [20], [19] proposed covert channels leveraging contention in *fsync* calls on shared persistent storage. In contrast, our work identifies an orthogonal leakage source by exploiting delay patterns in *syncfs*. The type of leakage exposed by *syncfs* is fundamentally different from contention-based leakages in that the leakage depends on the write behavior of the victim. Thus, unlike *fsync*-based methods, our approach does not rely on the victim application executing any *fsync* calls; the victim simply writes data

to the file system. This leakage is significantly richer than contention leakage, enabling both robust covert channels and high-resolution side-channel attacks. In particular, our threat model assumes a malicious application or process without special privileges, aiming to infer sensitive information about other applications sharing the file system. When the attacker invokes *syncfs*, it flushes not only its own dirty pages but also the pending changes from other applications. By analyzing the timing delays of *syncfs*, the attacker infers the I/O patterns of these processes. For example, *syncfs* delays increase when other applications perform more writes to the unflushed page caches, such as during webpage loading, video streaming, or the launch of an Android application.

In this work, we first identify two novel leakage vectors through the *syncfs* system call (illustrated in § 3). First, we demonstrate how *syncfs* can profile I/O system call footprints, revealing the impact of various I/O operations on execution delays. Second, we show that *syncfs* leakages can infer file write sizes, with latency patterns varying linearly below 4 KB and exhibiting dynamic behavior above 4 KB due to kernel optimizations.

We then build up a covert channel attack by leveraging *syncfs*-based leakage vectors (illustrated in § 4). By exploiting delay patterns of *syncfs*, the attacker encodes information into binary bits, with high delays representing "1" and low delays representing "0". The synchronization mechanism relies on the Time Stamp Counter (TSC) for precise timing coordination between the sender and receiver. Experiments on various Linux file systems (e.g., ext4, ext2, and xfs) and the Windows NTFS file system reveal bandwidths up to 7.61 Kbps with error rates ranging from 0.01% to 1.9%.

We also exploit leakage vectors of *syncfs* to develop three end-to-end side-channel attacks (illustrated in § 5). These attacks infer sensitive user activities, such as website visits, video streams, and application launches, on Linux and Android devices. By analyzing the timing patterns of *syncfs*, our attacks reveal distinct footprints for these activities. To enhance the effectiveness of our attacks, we employ the Short-Time Fourier Transform (STFT) to extract frequency-domain features from the timing data. These features are further processed using a Convolutional Neural Network (CNN) model. For website fingerprinting, we identify unique *syncfs* delay patterns caused by file writes during website loading, achieving an F1 score of over 93% in both closed- and open-world scenarios. Similarly, video fingerprinting leverages timing differences from buffering operations, demonstrating high accuracy across streaming platforms like YouTube and Bilibili. In closed-world evaluations, our approach achieves F1 scores exceeding 95% for YouTube and 89% for Bilibili. Even in open-world settings, our method maintains robust performance, achieving F1 scores of 92.74% for YouTube and 87.03% for Bilibili platforms. On Android devices, application fingerprinting exploits write patterns during app launches, achieving an average F1 score of over 93%.

In our final attack, we adapt the *syncfs*-based attack to containerized environments, targeting both detection and covert communication. By monitoring *syncfs* delays, our

container detection technique identifies mount and unmount operations associated with container startup and shutdown. These operations create distinct delay spikes, enabling precise identification of container activity. Furthermore, we construct a cross-container covert channel where separate containers communicate by encoding data into *syncfs* delay patterns. Despite the added noise and virtualization overhead inherent in container environments, the attack achieves a bandwidth of 0.23 Kbps with an error rate of 2.4%.

In summary, the contributions of this paper are:

- *New attack vector.* We analyze the *syncfs* system call on Linux and Android, identifying timing leakages that serve as a novel attack vector.
- *Covert channel attack.* We design and implement a fast, resilient covert channel leveraging *syncfs*, demonstrating its effectiveness across Linux and Windows file systems.
- *End-to-end side channel attacks.* We present three high-accuracy side-channel attacks to infer visited websites, streamed videos, and foreground applications, achieving over 90% performance in precision, recall, and F1 score.
- *Cross container attacks.* We extend the *syncfs* attack to containerized environments, demonstrating both container detection and a cross-container covert channel with practical feasibility.

## 2. Background and Threat Model

This section begins with an overview of the Linux file system and I/O buffers. Next, we explain the key system calls relevant to I/O operations. Finally, we present our threat model.

### 2.1. Linux File System

The Linux file system is a hierarchical framework that organizes, stores and retrieves data on physical storage devices. It acts as a bridge between user applications and the physical device, enabling efficient and reliable data management across Linux systems [21].

Figure 1 shows the structure of the Linux file system, highlighting the flow of I/O system calls from the application layer to the physical device. The architecture has multiple layers, each with distinct responsibilities. At the top is the **application layer**, where user applications interact with the file system through libraries like the GNU C Library. These interactions result in system calls, such as *read*, *write*, *rename*, and synchronization calls like *syncfs* or *fsync*. These system calls are the foundation of file operations.

Beneath the application layer, the **Virtual File System (VFS)** serves as an abstraction layer in the kernel. It standardizes file access, allowing applications to work with files without knowing the details of the underlying file system. This design enables efficient support for multiple file systems, including ext4, XFS, and btrfs, each optimized for different use cases. The VFS bridges the gap between user

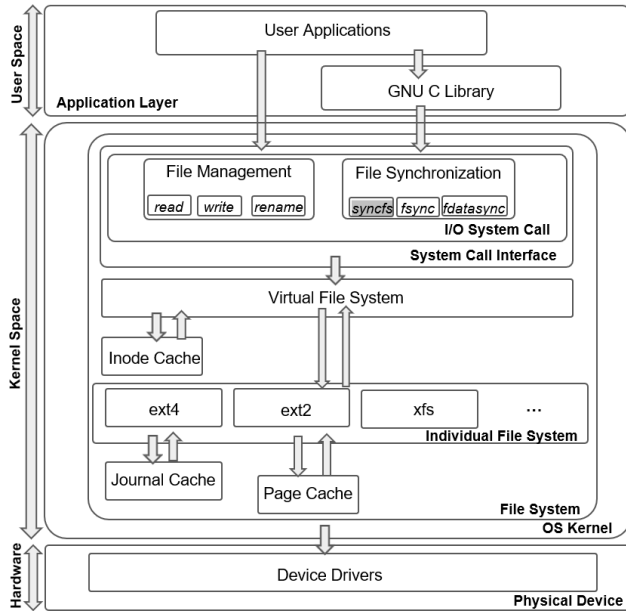


Figure 1: Overview of Linux file system and I/O system calls between the application layer and the physical device.

operations and the specific implementation of individual file systems.

Among these file systems, ext4 is the general-purpose choice and is often set as the default for most Linux installations due to its stability and versatility [32]. Ext4 provides efficient storage management, large file support, and backward compatibility with earlier file systems like ext2 and ext3. Additionally, its journaling feature enhances reliability by tracking changes before committing them to disk, protecting data in the event of a system crash. For specialized needs, alternative file systems are available. XFS focuses on high-performance workloads with efficient parallel I/O operations, making it ideal for servers and data-intensive applications [33]. Btrfs emphasizes enhanced data integrity with built-in redundancy and snapshots, which are particularly valuable for environments requiring robust data protection [34]. Finally, NFS supports networked file sharing, enabling seamless access to files across distributed systems [35]. Each of these file systems provides distinct features tailored to specific requirements.

The next layer consists of the actual file systems and their caching mechanisms. These include the **inode cache**, which stores file metadata, the **page cache**, which buffers file data, and the **journal cache**, which tracks transactional logs to ensure data integrity. These caches improve performance by minimizing direct disk access, allowing the system to process file operations more quickly.

Finally, at the bottom of the stack, **device drivers** handle communication with the physical device. They execute the low-level commands needed to complete read and write requests.

## 2.2. Linux I/O Buffers

**Inode cache.** The inode cache is a memory-resident structure in the main memory that stores recently accessed inodes, which are data structures containing metadata about files and directories. Its purpose is to bypass disk reads and writes, thereby reducing latency and speeding up common I/O operations. This caching mechanism plays a critical role in optimizing file system performance.

**Page cache.** The page cache in Linux is an in-memory structure that stores filesystem data to accelerate access. Acting as a buffer, it holds copies of data to enhance system responsiveness and overall performance. When modified, a cached page becomes a "dirty page," requiring eventual write-back to the physical device. The page cache can utilize all available memory, but it dynamically releases memory when needed by other processes. A background process handles the write-back mechanism for dirty pages. Additionally, user applications can trigger write-backs using I/O system calls such as *fsync*, *sync*, *syncfs*.

**Journal cache.** The journal cache is a dedicated memory area used by journaling file systems to temporarily store updates to the file system's journal before committing them to disk. This mechanism enhances reliability and performance by capturing file system changes in memory. During file operations, the file system logs transaction metadata in the journal cache. Journaling typically follows one of two approaches: metadata journaling, which logs only file system metadata, and full journaling, which records both data and metadata.

## 2.3. System Call for I/O

**File management system calls.** System calls for I/O are essential functions that allow user programs to interact with the kernel to perform I/O operations. Common I/O system calls include *open*, *read*, and *write* to transfer data between the disk and the program memories. Applications commonly use these I/O system calls due to its functionality and low overhead.

**File synchronization system calls.** Synchronization system calls allow manual synchronization of pending changes in I/O buffers. Commonly used calls include *fsync* and *fdatsync*, which flush dirty pages from I/O buffers associated with individual files. In this paper, we focus on the Linux system call *syncfs*. Unlike other synchronization calls, *syncfs* operates at the file system level. It flushes all dirty pages related to the file's superblock, synchronizing every file within the disk partition to the physical device.

***syncfs* workflow.** *syncfs* consists of three main components: synchronizing inodes, synchronizing data, and performing file system-specific operations. Each component uses a lightweight function to initiate the write-back process, followed by a blocking function that ensures the operations are complete.

For inode synchronization, the function `writeback_inode_sb()` marks inodes as dirty and initiates write-back without waiting, while

`sync_inode_sb()` ensures all dirty inodes are flushed to disk. This approach extends to data synchronization as well.

The function `sync_blockdev_nowait()` sends write-back requests and returns immediately. At the end of `syncfs`, `sync_blockdev()` is called in a loop to flush all dirty pages, incorporating an I/O throttling mechanism to periodically put the process to sleep. This throttling prevents the physical device from becoming overwhelmed and avoids saturating the I/O bandwidth.

File system-specific operations depend on the implementation of each file system. File system-specific operations vary based on the implementation of each file system. A representative example is `sb->s_op->sync_fs()`, which handles synchronization tasks unique to the file system’s design. In ext4, this operation records metadata to the journal to maintain data consistency. Finally, `blkdev_issue_flush()` flushes the physical device’s internal cache, guaranteeing that the journal log is physically written to the disk.

## 2.4. Threat Model

Our threat model assumes that a *spy* application and a *victim* application execute on the same shared file system. In Linux or Windows, it is common for all applications to operate within the same file system, especially in standard desktop and server installations. We do not assume the spy has superuser privileges or access to specialized hardware. The spy operates as a regular user and periodically invokes the `syncfs` system call, which requires no root permissions. The only requirement is a Linux kernel version 2.6.39 or higher, or an Android OS version 9 or later, both of which support the `syncfs` system call.

The spy initiates the attack by repeatedly calling `syncfs` in a loop to clear the page cache as preparation. It continuously calls `syncfs` in the background while recording the system call’s time delay. When the victim process runs, any I/O system calls it performs that modify data or metadata increase the delay observed by the spy. The spy analyzes this delay pattern to infer the victim’s file system activities.

Our attacks generalize to most file systems, including both native and non-native file systems on Linux and Android. Variations in the implementation of file system-specific operations within `syncfs` may cause its performance to differ across file systems. In the covert channel attack, the sender performs distinct file system operations to encode bits "0" and "1". The receiver continuously invokes `syncfs` in the background to detect these signals. By measuring the differences in `syncfs` delays, the receiver decodes the transmitted message. In the side-channel attack, the attacker flushes the page cache at the file system level to monitor the victim’s I/O operations. For fingerprinting attacks, the attacker captures the victim’s write patterns and leverages them to classify user activities. Specifically, in the Android application fingerprinting attack, the attacker records the I/O activities of applications during boot-up to identify them.

## 3. Leakage Vectors through `syncfs`

In this section, we introduce a *new* attack vector on the Linux file system via `syncfs`. We demonstrate how `syncfs` can be leveraged to profile the footprints of other Linux I/O system calls. Additionally, we focus on the `write` system call and show that the written file size can be inferred using `syncfs` leakages.

### 3.1. Measuring I/O System Call Footprint via `syncfs`

The `syncfs` system call operates at the file system level rather than on individual files. It ensures that all dirty data and metadata in the file system are flushed to the storage device. In ext4, `syncfs` flushes **dirty inodes, dirty pages, and the journal**. We observed that the execution time of `syncfs` increases when the file system has pending changes in these I/O buffers caused by other operations (*e.g.*, `write` and `ftruncate`).

#### Experiment 1: I/O operations delay `syncfs` execution.

Our first experiment tests the delay impact on `syncfs` caused by different I/O operations. We selected four operations that introduce delays in `syncfs`: `write`, `ftruncate`, `write(O_SYNC)`, and `rename`. These operations affect different I/O buffers, as summarized in Table 1:

- Operation `write` appends or updates data asynchronously to a file, affecting the page cache, journal cache, and inode cache.
- Operation `write(O_SYNC)` writes data synchronously, affecting only journal cache.
- Operation `ftruncate` adjusts the file size (truncate or extend), impacting the inode cache and journal cache.
- Operation `rename` changes a file’s name, modifying the journal cache and inode cache.

**Experiment platform.** We use an NVIDIA Jetson AGX Orin machine with the ext4 file system set to default and a kernel version of 5.15.136-tegra. To measure timing, we use the ARM Generic Timer counter register, `CNTVCT_EL0` [36]. We execute each I/O operation followed by a `syncfs` call to measure its impact on delay. For `write`, we write a full data block (4 KB) to a file, adding dirty pages and inodes to I/O buffers. The `syncfs` delay includes the extra time to flush the page cache, inode cache, and journal log. To test `ftruncate` and `rename`, we shrink a file size to 0 and rename a file, respectively. These two operations modify only metadata, adding dirty inodes to the buffer. The `syncfs` delay reflects flushing the inode cache and journal log. For `write(O_SYNC)`, we set the `O_SYNC` flag and write a full data block (4 KB) synchronously. Since data and metadata are directly written, `syncfs` only needs to flush the journal log. Additionally, we measure the base delay of `syncfs` as the baseline, representing its execution time without any I/O processes.

**Results.** We measure the latency of each operation 1,000 times and calculate the average and standard deviation.

TABLE 1: *syncfs* leakages for different I/O operations.

I/O operation	Affected buffers	Average latency (cycles)	Standard deviation
baseline	N/A	2509	491
write	Page cache, journal and inode	121092	11436
write(O_SYNC)	journal	41406	4670
ftruncate	journal and inode	61315	6916
rename	journal and inode	66774	8134

Table 1 summarizes the results. Compared to the baseline, all four operations increase the *syncfs* latency by at least 16 times. Among them, *write* introduces the highest latency, averaging 121,091 clock cycles, as it affects three buffers: the page cache, journal, and inode cache.

In contrast, *write(O\_SYNC)*, which only updates the journal log, incurs the lowest latency, averaging 41,406 clock cycles. Operations *ftruncate* and *rename* both modify the journal and inode cache, resulting in average latencies of 61,315 and 66,774 clock cycles, respectively.

**Observation 1:** I/O operations delay *syncfs* execution time, with different operations causing varying impacts on *syncfs* latency.

**Experiment 2: impact of concurrent I/O operations on *syncfs* latency.** Our first experiment analyzed the impact of a single I/O operation on *syncfs* latency. However, in real-world scenarios, multiple I/O operations are more likely to be executed concurrently to handle multiple files. For example, several files might be renamed, truncated, or written simultaneously. Thus, our second experiment measures the latency impact on *syncfs* caused by concurrent I/O operations.

**Experiment platform.** This experiment is conducted on a Linux PC with an Intel Xeon E5-2698v4 CPU running Ubuntu 20.04. We use the unprivileged *rdtsc* timer to measure latency on the ext4 file system. The tested I/O operations in this experiment include: *write(64B)*, *write(O\_SYNC)(64B)*, and *ftruncate(0)*, as detailed below:

- Operation *write(64B)*: Writes 64 bytes of data to a file using the standard *write()* system call.
- Operation *write(O\_SYNC)(64B)*: Writes 64 bytes of data directly to the disk, bypassing the OS’s page cache.
- Operation *ftruncate(0)*: Truncate a file of 64 bytes to 0 bytes.

In this experiment, we measure the *syncfs* delay caused by flushing extra dirty buffers generated by three I/O system calls while increasing the number of files to process. Figure 2 shows the delay patterns for *write(64B)*, *write(O\_SYNC)(64B)*, and *ftruncate*. We observe that the *syncfs* delay for all three I/O system calls increases as the file

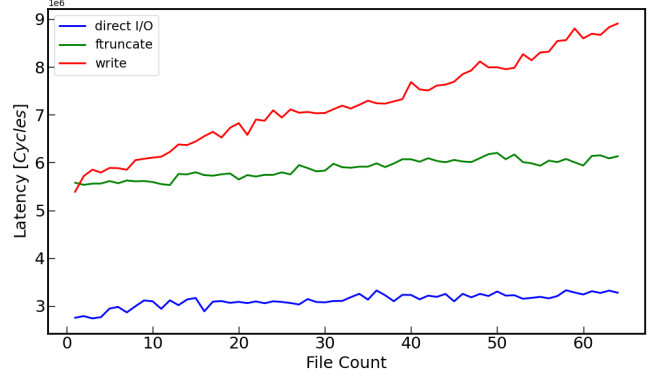


Figure 2: *syncfs* delay of concurrent I/O system calls on ext4

count grows, but with varying slopes. The calculated slopes of the delay patterns are 6,163 (*write(O\_SYNC)*), 9,626 (*ftruncate*), and 48,612 (*write*), reflecting the differences in overhead caused by each operation.

For direct I/O (*write(O\_SYNC)(64B)*), the *syncfs* latency increases slightly, even with multiple concurrent operations, as this call primarily affects the journal cache. Similarly, the latency of *syncfs* shows a modest increase for concurrent *ftruncate* operations, which generate additional dirty journal and inode entries for flushing. In contrast, the *write* operation, which affects the journal, inode, and page cache, causes a steep linear increase in *syncfs* latency as the number of processed files increases. Additionally, extra inode entries, journal updates, or dirty pages cannot be merged by the I/O scheduler. As the scheduler serializes the write-back requests, the resulting overhead leads to progressively longer delays for *syncfs*.

**Observation 2:** An increasing number of I/O operations also increases *syncfs* delay. Different operations have varying degrees of impact on the growth of *syncfs* latency.

### 3.2. Inferring *write* Size via *syncfs*

**Motivation.** Among these I/O system calls, *write* is most frequently used in both application and system-level programs. It is essential for writing various outputs. The size parameter in *write* directly specifies the number of bytes to be written from a buffer to a file. It can always reflect the actual size of the object being written to a file. Therefore, in this experiment, we explore whether *syncfs* can leak the write size of a *write* system call.

**Experiment 3: infer write size via *syncfs*.** We have two steps for this experiment: within page size (4KB), and above page cache size. Within page size, we set the initial write size as 64 bytes. It keeps increasing with a stride of 64 bytes and ends at 4 KB. Above page size, we set the initial write size as 4 KB. It keeps increasing with a stride of 4 KB and ends at 64 KB. The experiment was conducted on an NVIDIA Jetson AGX Orin machine with the ext4 file

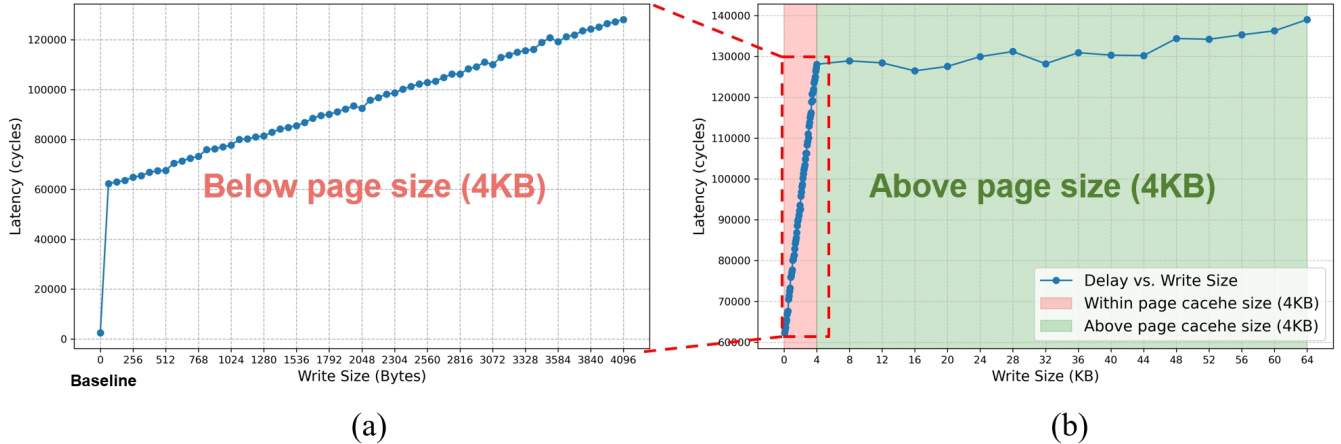


Figure 3: *syncfs* latency with different *write* size: (a) Below page size (4KB), (b) Above page size (4KB).

system set to default and running kernel version 5.15.136-tegra.

**Results when below the page size.** Figure 3 (a) shows the zoomed-in *syncfs* latency for write sizes ranging from 64 bytes to 4,096 bytes. The baseline latency, when no write occurs, is approximately 2,000 cycles. However, at a write size of 64 bytes, there is a significant jump in latency to around 62,000 cycles.

As the write size increases within the page size limit (4 KB), the *syncfs* latency grows linearly. This is because larger write sizes generate more dirty page cache entries, journal updates, and inode changes, leading to longer flushing times for *syncfs*. Specifically, *syncfs* performs I/O in two stages: `sync_blockdev_nowait()`, which initiates a write-back request, and `sync_blockdev()`, which loops until the write-back completes. As the write size grows, `sync_blockdev()` takes longer to exit the loop. Within this loop, periodic I/O throttling forces the process to sleep for a fixed duration, further increasing delays. These cumulative delays result in the observed linear relationship between write size and *syncfs* latency.

**Results when above the page size.** However, when the write size exceeds 4 KB, the increase in *syncfs* latency slows down significantly, as shown in Figure 3 (b). This slowdown is due to parallelism in the I/O process. When the write size exceeds 4 KB, dirty pages are merged and processed by multiple flusher threads [37].

We also observe more fluctuations in the latency pattern for write sizes above 4 KB. This is primarily caused by the kernel’s dynamic adjustment of flusher threads, which are responsible for writing dirty pages back to the physical disk [38]. The Linux kernel adjusts the number of flusher threads based on factors such as system load and memory pressure. As a result, *syncfs* delay does not consistently increase with larger write sizes above 4 KB. While the fluctuations make the pattern noisy, it is still possible to infer the approximate range of write sizes beyond 4 KB.

**Observation 3:** For write sizes below 4 KB, *syncfs* latency grows linearly. For write sizes above 4 KB, *syncfs* latency slows due to I/O parallelism, with fluctuations from dynamic flusher thread adjustments.

## 4. Covert Channel Attack

In this section, we exploit the findings from Section 3 to build a fast and resilient covert channel. In Section 4.1, we describe the design of the covert channel and synchronization mechanisms. We evaluate and show results in Section 4.2.

### 4.1. Covert Channel Design

In this section, we outline the design of the covert channel. We assume the receiver (spy) and sender (trojan) processes operate on the same file system, sharing the same permission level as other normal processes.

**Covert channel synchronization.** A key component is the synchronization between the sender and receiver, as it significantly enhances bandwidth and reduces the error rate. We follow the synchronization method proposed in prior work [1]. As illustrated in Figure 4, we utilize the TSC (Time Stamp Counter) to synchronize the sender and receiver. Since TSC is a register timer accessible to any process, the current TSC value is shared between the sender and receiver. The sender and receiver both compute a start time by adding a predefined constant to the current TSC value. They wait until the computed start time, after which the sender begins transmitting the message with a starter code. Once the receiver detects the starter code, the covert channel is established.

**Design.** In the Section 3, we have observed that multiple I/O system calls can cause delay in *syncfs*. The communication channel based on *syncfs* leverages the write + flush mechanism in I/O buffers. The sender controls a file and writes data or metadata to it, marking dirty pages in the

---

**Algorithm 1** Receiver for Covert Channel

---

```
1: // curr_TSC is the current TSC value
2: // Pattern_receiver[N] is an array of N samples to record
   the delay pattern
3: // Message_receiver is a vector to store the parsed bits
4: // fd is a file controlled by the receiver
5: // T is the threshold to differentiate bits '1' and '0'
6: Synchronization(curr_TSC);
7: for  $i \leftarrow 0$  to  $N - 1$  do
8:    $start \leftarrow clock()$ ;
9:    $syncfs(fd)$ ;
10:   $end \leftarrow clock()$ ;
11:  // Check for the ending code
12: end for
```

---

I/O buffers. To minimize overhead, the sender uses direct I/O (`write(O_SYNC)`), which requires only the journal cache to be flushed. The receiver observes a higher `syncfs` delay when flushing the dirty pages. Conversely, when the sender is inactive, the receiver experiences the base `syncfs` delay, which occurs without any I/O operations.

The algorithms for the receiver and sender are visualized in Algorithm 1 and 2, respectively. Once synchronization via TSC is completed, the receiver begins measuring the delay of `syncfs`. It decodes the observed delay patterns into bit representations, stopping when it detects the ending code, a specific pattern indicating the end of the message.

We define bit '0' and bit '1' using distinct delay patterns, as shown in Algorithm 1. A higher delay caused by flushing I/O buffers represents bit '1', while a base delay without I/O represents bit '0'. In our covert channel, the sender adjusts the delay pattern by either writing 64 bytes to a file using direct I/O or executing a NOP loop for a defined number of iterations.

## 4.2. Covert Channel Evaluation

We evaluate the `syncfs` covert channel attack with two metrics: bandwidth and error rate. The bandwidth is measured in Kb per second, and the error rate is measured with Levenshtein edit distance [39].

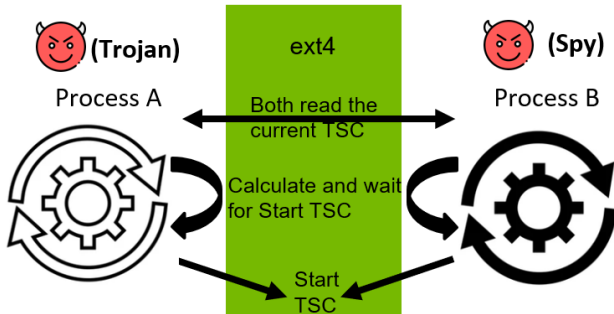


Figure 4: The `syncfs` covert channel uses TSC for synchronization on ext4 before transmission.

---

**Algorithm 2** Sender for Covert Channel

---

```
1: // Message_sender[N] is an array of N bits used to send
   a message
2: // fd is a file controlled by the sender
3: // R is the number of iterations to wait for flushing
4: // K is the number of iterations of no operation
5: Synchronization()
6: for  $i \leftarrow 0$  to  $N - 1$  do
7:   if  $D_{sender}[i] == 1$  then
8:      $write(fd, string, size)$ ;
9:     for  $j \leftarrow 0$  to  $R - 1$  do
10:      NOP;
11:    end for
12:   else
13:     for  $j \leftarrow 0$  to  $K - 1$  do
14:      NOP;
15:    end for
16:   end if
17: end for
```

---

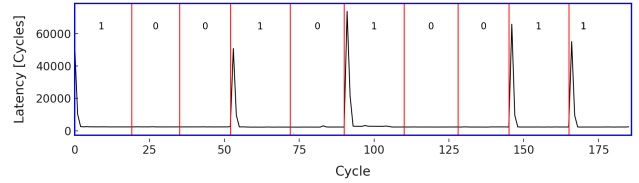


Figure 5: The `syncfs` covert channel transmission has a clear difference between bit '0' and '1' on ext4.

**Covert channel demonstration.** Figure 5 illustrates our covert channel on the ext4 file system, where the distinct latency pattern of `syncfs` encodes data: higher latency represents bit "1," while lower latency represents bit "0."

**Linux file system.** We implement the covert channel on multiple file systems, including ext4, ext2, and xfs, and evaluate it based on bandwidth and error rate, as summarized in Table 2. Due to the higher average latency of `syncfs`, we achieve the lowest bandwidth of 0.94 Kbps with an error rate of 0.01% on ext4. On ext2, the bandwidth reaches 3.28 Kbps, but with a higher error rate of 1.6%, attributed to increased background noise. On XFS, we achieve the highest bandwidth of 4.98 Kbps with a moderate error rate of 0.15%.

**Windows file system.** We also explore the scenario of running Linux on a Windows machine, such as using WSL, which provides a lightweight Linux environment [40]. In this setup, the Linux system operates on the NTFS file system via the NTFS3 driver. Implementing the `syncfs` covert channel on NTFS achieves the highest bandwidth of 7.61 Kbps with a 1.9% error rate. The increased bandwidth compared to Linux native file systems is due to the significantly lower `syncfs` delay for direct I/O operations.

## 5. Side Channel Attacks

In this section, we utilize the leakage vectors identified in Section 3 to design three side-channel attacks:

TABLE 2: Covert channel results: Bandwidth (Kbps), and Error rate (%).

	Bandwidth	Error rate
ext4	0.94	0.01
ext2	3.28	1.6
xf	4.98	0.15
ntfs	<b>7.61</b>	1.9

website fingerprinting, video fingerprinting, and application fingerprinting. We assume a malicious process continually profiles timing side-channel leakage through *syncfs* while a victim process visits a website, watches a video, or launches an application. This approach enables the identification of the specific website, video, or application accessed by the victim. The website and video fingerprinting attacks are demonstrated on Linux file systems (Section 5.1 and Section 5.2), while the application launch identification attack (Section 5.3) is conducted on Android devices.

### 5.1. Attack 1: Web Fingerprinting on Linux

In this attack, we demonstrate that an attacker can infer the specific website visited by the victim user in a closed-world setting over the top 100 websites from the Alexa top 1 million list [41] and an open-world setting with the top 100 websites and an `other-class` for websites that not listed in the top 100 websites.

**Experimental setup and attack overview.** We run our experiments with the Chrome browser (Version 124.0.6367.201) on an i7-11800h CPU and Ubuntu 20.04. We assume the attacker is a normal user on that machine and can access the unprivileged *rdtsc* timer and *syncfs* system call. The system configurations are all in default with the ext4 file system. The attack and the victim co-locate on the main partition of the disk that is running the ext4 file system. We assume the victim Chrome browser has browser cache enabled as default.

Our attack consists of two main stages: an online data collection phase and an offline phase for data preprocessing and trace evaluation. In the online phase, the attacker profiles the file system’s write pattern in the background while the victim loads a website. As the website loads, the browser requests necessary files from the server and stores them in its cache. These temporary cache files are often partially encrypted and have limited user access. Although Chrome isolates each tab or process in a sandboxed environment to protect its cache, the browser cache files still share the page cache with other processes. Each website has a unique *syncfs* delay pattern due to its specific write frequency and object sizes.

#### Observing STFT distinguishability and classification.

To process the data, we apply the short-time Fourier transform (STFT) [42] on the traces with a window size of 256 to capture frequency information. STFT highlights how frequency components change over time, refining signal analysis [1], [43], [44]. Using the *scipy* package [45],

we implement STFT and present the results in Figure 6, showing traces for `google.com`, `netflix.com`, and `reddit.com`. The x-axis represents sample numbers, with each trace containing 50,000 samples, while the y-axis indicates frequency changes. Observing the STFTs of these websites reveals clear distinguishability, enabling us to classify them by feeding these STFT images into a convolutional neural network (CNN).

We use the ResNet-152 CNN model [46] with pre-trained weights, customizing the first layer to accept a single input channel for our grayscale STFT images. The STFT images are resized to 224 by 224 pixels, and we train and evaluate the model in PyTorch [47] version 2.1.2 using 10-fold cross-validation [48]. For each fold, we evaluate performance using three metrics: F1 score (F1), Precision (Prec), and Recall (Rec). Our training setup utilizes the *CrossEntropyLoss* function for multi-class classification and optimizes using the *Adam* optimizer with a learning rate of 0.0001 and weight decay of  $1e-5$ .

**Evaluation in close-world setting.** We collect 10,000 traces (100 per website) for a closed-world attack, resulting in 100 STFT images per website. The last layer of ResNet-152 is set to 100 classes, and the model is evaluated on an NVIDIA Tesla V100 GPU. We use a batch size of 80 for both training and evaluation. Table 3 presents the performance of our side-channel attack on website fingerprinting. The average F1 score across 10 folds is 93.82%, with a standard deviation of 6.96%. Precision averages over 94%, with a standard deviation of 5.58%, while recall reaches an average of 93.77%, with a 7.09% standard deviation across 10-fold cross-validation.

**Evaluation in open-world setting.** The classification results reported in previous sections were based on datasets collected in a closed-world setting (100 traces for each of the Alexa top 100 websites). To evaluate our attack in an open-world setting, we collected additional traces following the methodology outlined in prior works [49], [1], [50]. The open-world dataset includes the closed-world data plus 5,000 randomly selected Alexa websites (1 trace per website). We used the same ResNet-152 model, adjusting the last layer to classify 101 classes. Table 3 presents our website fingerprinting attack’s performance in the open-world setting. The average F1 score across 10 folds slightly decreases from 93.82% to 93.25%, with a standard deviation of 6.79%, due to the addition of the new `other-class`. Precision remains above 94%, with a standard deviation of 5.42%, and recall averages 93.25%, with a standard deviation of 6.67% across 10-fold cross-validation.

**Comparison with Sync+Sync [20].** Jiang et al. [20] introduced *fsync*-based contention leakage for website fingerprinting, requiring both the victim and attacker to use the *fsync* system call to create contention. Their approach, however, is limited by the similar number of *fsync* calls across websites, resulting in low accuracy for website fingerprinting, with reliable identification for **only two** websites (`qq.com` and `sina.com.cn`). In contrast, our method utilizes each website’s unique *syncfs* delay pattern, which reflects specific write frequencies and content sizes. It im-



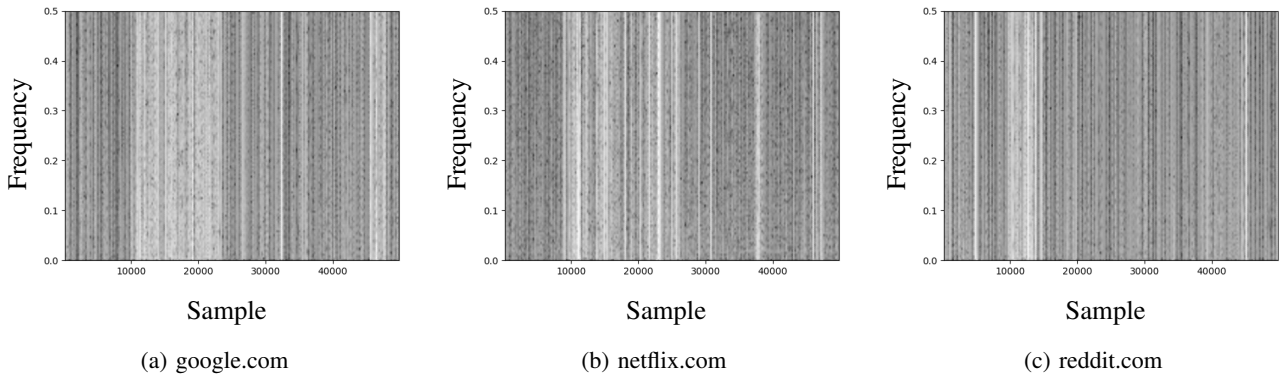


Figure 6: The STFTs of side-channel traces collected during the victim’s access to different websites show distinct patterns for (a) google.com, (b) netflix.com, and (c) reddit.com.

TABLE 3: Web fingerprint performance: F1 (%), Precision (%), and Recall (%).

	F1	Precision	Recall
	$\mu(\sigma)$	$\mu(\sigma)$	$\mu(\sigma)$
Close world	93.82 (6.96)	94.99 (5.58)	93.77 (7.09)
Open world	93.25 (6.79)	94.67 (5.42)	93.25 (6.67)

poses no special requirements on the victim user’s behavior (e.g., *fsync* calls). Our approach achieves over 93% average F1 score for 100-class website fingerprinting.

## 5.2. Attack 2: Video Fingerprinting on Linux

In this attack, we demonstrate that an attacker can infer the specific video played by the victim in a closed-world setting across the top 20 videos from two platforms: YouTube (`youtube.com`) and Bilibili (`bilibili.com`) trending lists. We also evaluate in an open-world setting, which includes the top 20 videos plus an `other-class` for videos not listed in the trending lists.

**Experimental setup and data collection.** In this attack, we conduct our experiments on an i7-11800h CPU with Ubuntu 20.04. We assume the attacker is a standard user on the machine with access to the unprivileged *rdtsc* timer and *syncfs* system call. Following the previous video fingerprinting attack setup, we use FFmpeg for live video streaming, as done in previous works [51], [52], [53], [54]. FFmpeg, an open-source audio and video converter, supports most industry-standard codecs, enabling efficient file format conversion [55].

In our attack, we assume the victim uses *ffplay*, a lightweight media player based on FFmpeg libraries, to watch video streams, while a separate host machine runs *ffmpeg* as the streaming server. Meanwhile, the attacker profiles the write patterns of the victim’s *ffplay* in the background. For smooth playback, *ffplay* uses internal buffering for network streams, with different video content producing distinct write patterns in this buffer. Consequently, the at-

tacker can fingerprint the victim’s video by profiling these write patterns via the *syncfs* system call.

### Observing STFT Differentiability and Classification.

Following our web fingerprinting attack’s preprocessing method, we use STFT to extract frequency-based features from time-series leakages collected via the *syncfs* system call. The STFT uses a window size of 256 to capture frequency information. Fig 7 shows the STFT images representing playback patterns for three videos when the victim streams them. The x-axis denotes sample numbers, with each trace containing 50,000 samples, while the y-axis represents frequency features. Observing these STFTs reveals clear differentiability, enabling the attacker to identify which video is playing on the victim’s device.

We use the same ResNet-152 CNN model as in our web fingerprinting attack, modifying the last layer to classify 20 classes. The model is evaluated using 10-fold cross-validation and three performance metrics: F1 score (F1), Precision (Prec), and Recall (Rec). Our training setup includes *CrossEntropyLoss* as the loss function and *AdamW* as the optimizer, with a learning rate of 0.0001 and weight decay of  $1e-5$ .

**Close-world setting.** We collect 2,000 traces (100 per video) for a closed-world attack, resulting in 100 STFT images per video. A batch size of 20 is used for both training and evaluation. Table 4 and Table 5 present the performance of our video fingerprinting attack across two platforms. On YouTube, the average F1 score across 10 folds exceeds 95%, with a small standard deviation of 7.64%. Precision averages 96.45%, with a standard deviation of 6.22%, while recall averages 95.68%, with a 7.63% standard deviation across 10-fold cross-validation. However, on Bilibili, the model performs slightly worse: the F1 score drops to 89.68%, with a higher standard deviation of 15.84%. Precision remains above 90%, with a standard deviation of 14.57%, and recall decreases to 89.80%, with a standard deviation of 15.54%. We conjecture that the difference in performance between the two platforms is due to video quality. On Bilibili, videos are played in low quality by default [56], whereas YouTube does not impose this constraint.

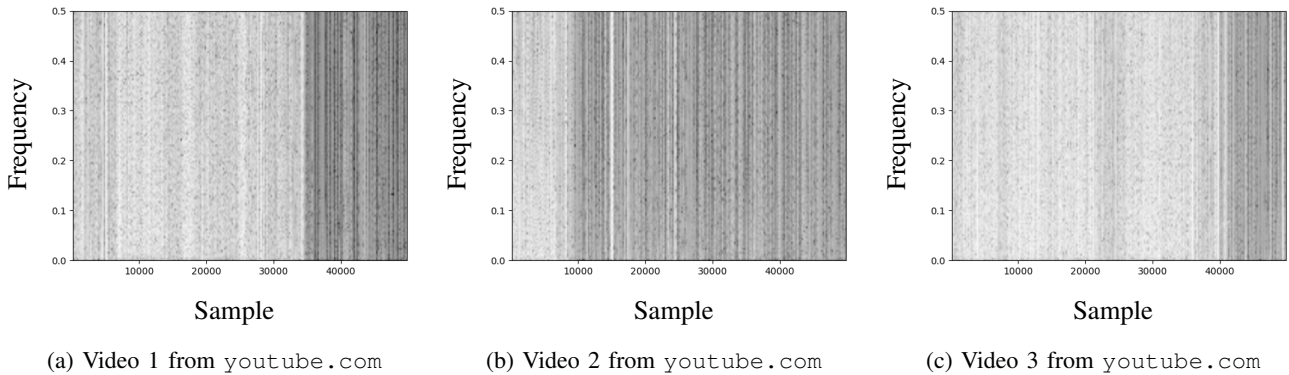


Figure 7: The STFTs of side-channel traces collected during the victim’s playback of different videos on `youtube.com` reveal distinct patterns for each of the three videos.

TABLE 4: Video fingerprint performance on Youtube: F1 (%), Precision (%), and Recall (%).

	<b>F1</b>	<b>Precision</b>	<b>Recall</b>
	$\mu(\sigma)$	$\mu(\sigma)$	$\mu(\sigma)$
Close world	95.69 (7.64)	96.45 (6.22)	95.68 (7.63)
Open world	92.74 (12.87)	94.70 (9.21)	92.69 (12.95)

TABLE 5: Video fingerprint performance on Bilibili: F1 (%), Precision (%), and Recall (%).

	<b>F1</b>	<b>Precision</b>	<b>Recall</b>
	$\mu(\sigma)$	$\mu(\sigma)$	$\mu(\sigma)$
Close world	89.68 (15.84)	90.87 (14.57)	89.80 (15.54)
Open world	87.03 (18.33)	89.26 (15.69)	87.26 (17.87)

**Open-world setting.** In addition to the top 20 videos in the closed-world setting, we add an `other-class` containing 50 randomly selected videos (1 trace per video). We retained the same ResNet-152 model, adjusting the last layer to classify 21 classes. Table 4 and Table 5 present the performance of our video fingerprinting attack in the open-world setting. On YouTube, the F1 score decreases by approximately 3%, with precision dropping around 2% and recall by 3% compared to the closed-world setting. On Bilibili, performance also decreases, but the F1 score still exceeds 87%, with precision reaching 89.26% and recall remaining over 87%.

### 5.3. Attack 3: Application Fingerprinting on Android

Information about other concurrent applications can reveal sensitive details about user activity and provide context for additional attacks, such as phishing [17] and keystroke inference [18]. In this section, we show that an attacker can identify specific applications launched by the victim from a set of 15 popular Android applications.

**Experimental setup and data collection.** In this attack, we conduct our experiments on a Samsung S20 running Android 14. We assume the attacker is a standard user on

this phone, with access to the unprivileged `clock_gettime` timer and `syncfs` system call. Following the setup of our previous fingerprinting attacks, we assume the victim launches applications in the foreground, while the attacker profiles the write patterns of these launches in the background. The sampling rate of the attacker’s profiler is around 150,000 cycles/sec. Since each application launch generates unique write patterns in the Android system’s page cache, the attacker can infer the victim’s application by monitoring these patterns through the `syncfs` system call. Table 6 lists the tested applications, all of which were downloaded from the Google Play Store. These apps represent the most popular choices within their respective categories.

Category	Application
Social & Entertainment	Bluesky, Instagram, Tiktok, X, Netflix, IMDB, Youtube, Genshin Impact
Shopping & E-commerce	Amazon, Temu
Travel & Services	Airbnb, Uber
Finance & Utilities	Wells Fargo, ChatGPT, Google Map

TABLE 6: Applications evaluated for the fingerprinting attack.

**Application fingerprinting demonstration and results.** We use STFT for data preprocessing to extract frequency-based features from time-series leakages collected via the `syncfs` system call. The STFT uses a window size of 256 to capture frequency information. Fig 8 displays STFT images representing the launch patterns of three popular Android applications: X, TikTok, and Uber. The x-axis denotes sample numbers, with each trace containing 600,000 samples, while the y-axis represents frequency features. Utilizing the new timer on the Android phone provides a higher sample rate than in the previous two attacks. This results in clearly differentiated STFT images, allowing us to identify which application is concurrently running on the victim’s device. We use the same ResNet-152 CNN model as in our web fingerprinting attack, modifying the last layer to classify 15

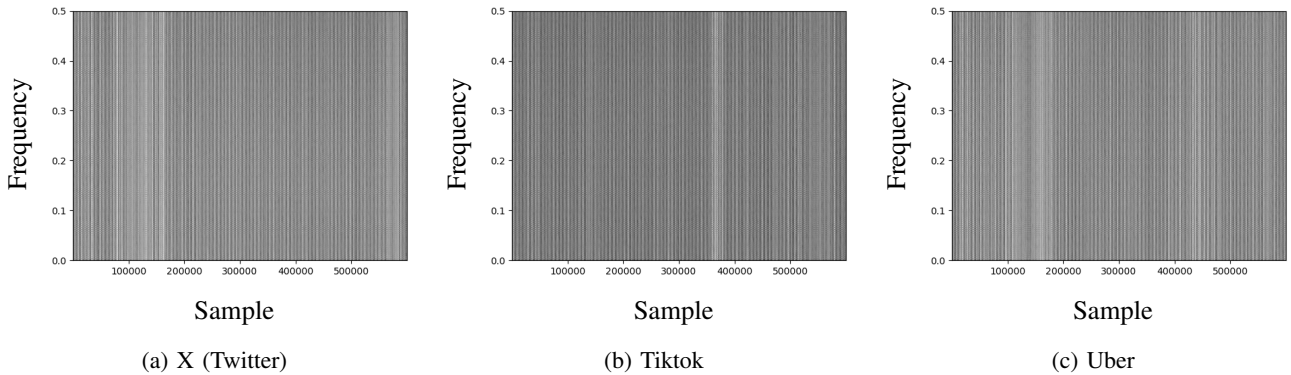


Figure 8: The STFTs of side-channel traces collected during the victim’s launch of different applications on an Android phone reveal distinct patterns for (a) X (Twitter), (b) TikTok, and (c) Uber.

TABLE 7: Application fingerprint performance on Android phone: F1 (%), Precision (%), and Recall (%).

	<b>F1</b>	<b>Precision</b>	<b>Recall</b>
	$\mu(\sigma)$	$\mu(\sigma)$	$\mu(\sigma)$
Android	93.49 (9.09)	95.13 (6.85)	96.62 (8.85)

classes. During training, we set *CrossEntropyLoss* as the loss function and *AdamW* as the optimizer, with a learning rate of 0.0001 and weight decay of  $1e-5$ . The batch size for both training and testing is set to 80.

Table 7 presents the performance of our application fingerprinting attack across 10 folds. The average F1 score is 93.49%, with a standard deviation of 9.09%. Precision averages 95.13%, with a standard deviation of 6.85%, while recall is over 96%, with a standard deviation of 8.85% across 10-fold cross-validation.

## 6. Cross-container Attack

Container technology is widely utilized by cloud computing service providers, such as Amazon Elastic Container Service (Amazon ECS) [57] and Google Cloud Platform (GCP) [58]. It offers a lightweight, operating system-level virtualization environment for efficient application hosting. In this attack, we investigate whether a spy can breach the isolation between two containers. In particular, we assume the spy resides in a separate container isolated from victim users, while these two containers share the same file system and hardware disks. The spy user continuously calls *syncfs* in her own container while recording its time delay. When the victim process runs, any I/O system calls it performs that modify data or metadata increase the delay observed by the spy. The spy analyzes this delay pattern to infer the victim’s file system activities.

**Attack setup.** We conduct our experiments on a Linux machine equipped with an Intel i7-11750H CPU, using the NTFS file system with the NTFS3 driver. The NTFS file system was chosen for its better bandwidth performance compared to native Linux file system formats, as presented

TABLE 8: *syncfs* leakages for different I/O operations in cross-container attacks.

<b>I/O operation</b>	<b>Affected buffers</b>	<b>Average latency (cycles)</b>	<b>Standard deviation</b>
baseline	N/A	1526882	243092
write	Page cache, journal and inode	19592860	2617313
write(O_SYNC)	journal	4854316	330761
fttruncate	journal and inode	10548983	1026260
rename	journal and inode	10616821	1729558

by our covert channel results in Table 2. We use Docker Engine v20.10.17 to create two containers on the Linux machine.

**Experiment 4: I/O operations impacts on *syncfs* execution in cross-container scenario.** In this experiment, we perform I/O operations in container A while measuring the execution time of *syncfs* in container B. Each operation is repeated 1,000 times, and the average and standard deviation of the *syncfs* execution time are calculated. Table 8 summarizes the *syncfs* delay caused by four different I/O operations. Compared to the baseline, all I/O operations increase *syncfs* delay by at least 3.1 times.

**Observation 4:** I/O operations delay *syncfs* execution time in **cross-container scenarios**, with different types of operations causing varying levels of impact on *syncfs* latency.

### 6.1. Detecting the Behavior of Container via *syncfs*

Containers must mount required directories during startup and unmount them when stopping, with these actions typically managed by the container runtime. In this section, we introduce a container detection technique leveraging

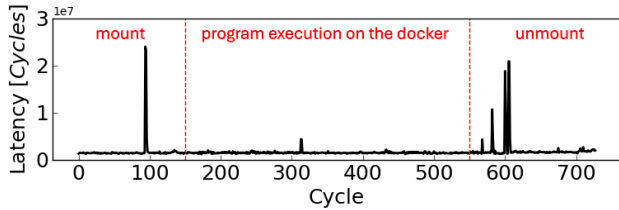


Figure 9: Detecting container startup and stop using *syncfs*.

*syncfs*. The spy user profiles the latency pattern of *syncfs* on container A while the victim user launches container B, mounts it to the file system, and runs a C program that sleeps for three seconds. Afterward, the victim stops container B and unmounts it from the file system. Figure 9 presents leakage traces collected by the spy on container A. Two distinct spikes, corresponding to the mount and unmount operations, indicate container B’s startup and shutdown, while the middle section represents the program execution.

Our detection method relies on lock contention, with the *s\_umount* semaphore, a reader-writer lock in the superblock data structure, playing a key role. When the attacker and victim share the same disk partition, lock contention arises. In this attack, *syncfs* acquires a reader lock during flushing, while mount and unmount operations acquire a writer lock. As a result, the spikes observed in the demo are caused by lock contention between these operations.

## 6.2. Cross-container Covert Channel Design

In a containerized environment, the sender and receiver are placed in separate containers, each managing a file within its working directory. We use the Timestamp Counter (TSC) as the synchronization method for the cross-container covert channel attack. Both the sender and receiver initialize a start TSC and begin transmitting messages once the current TSC matches the start TSC. The synchronization method is illustrated in Section 4.1.

To initiate the transmission, the sender transmits a predefined starting code to mark the beginning of the message. For data encoding, the sender uses direct I/O (*write(O\_SYNC)*) to add a transaction to the journal cache to represent a bit “1” and executes a no-operation loop to represent a bit “0”. We select *write(O\_SYNC)* since its average latency is lowest among four operations as shown in Table 8.

Simultaneously, the receiver repeatedly calls *syncfs* in a loop, analyzing the *syncfs* delay pattern to capture and decode the transmitted message. An ending code is appended to signify the termination of the message.

## 6.3. Cross-container Covert Channel Evaluation

We then evaluate the cross-container covert channel in terms of bandwidth and error rate. In this attack, we achieve a bandwidth of 0.23 Kbps with an error rate of 2.4%. The bandwidth of the cross-container covert channel is

significantly lower compared to the standard covert channel described in Section 4. This reduction is attributed to the virtualization overhead introduced by Docker. For example, the baseline execution time of *syncfs* in the cross-container scenario (when no other I/O operations are performed) is 1,526,882 cycles, which is over 600 times longer than in the same container scenario (2509 cycles as presented in Table 1).

## 7. Potential Mitigations

We propose four general classes of mitigations: (1) redesigning the *syncfs* system call, (2) restricting access to high-resolution timers, (3) detecting suspicious system call queries, and (4) supporting isolation in I/O buffers.

**Redesigning *syncfs*.** Completely blocking access to *syncfs* could serve as an effective defense against our attacks. However, this would also disrupt legitimate users who depend on *syncfs* to flush multiple file updates to disk. An alternative approach is to limit the frequency of *syncfs* calls, which could diminish the effectiveness of spy applications [11], [16]. Nonetheless, this strategy might impact legitimate users by potentially reducing *syncfs* functionality and weakening persistence against system failures. Fig. 10 shows the effect of reduced call frequency on application fingerprinting accuracy in Android. We observe that reducing the sampling frequency from 150,000 to 15,000 Hz causes the attack’s F1 score to drop significantly, from 93.49% to 32.99%. Further limiting the sampling rate to just 15 Hz reduces the attacker’s F1 score to 8.1%, which is nearly equivalent to random guessing (approximately 6.6%, given the application fingerprinting involves 15 classes). However, since *syncfs* plays a critical role in failure recovery, limiting the frequency of *syncfs* queries may introduce drawbacks, such as an increased risk of data loss or a higher likelihood of file system inconsistencies [59], [60].

In addition, since *syncfs* flushes the entire uncommitted page cache to the disk, a redesign to restrict users to flushing only their own page caches could mitigate the risk of cross-application data leakage. Another direction is to leverage hardware support, such as Physical Unclonable Functions (PUFs) [61], [62] and Trusted Execution Environments (TEEs) [63], to conceal timing leakages.

**Managing access to high-resolution clock instructions.** Our attacks rely on the high-resolution clock instructions, such as *CNTVCT\_ELO* and *rdtsc* timers, to measure the delay timing of *syncfs*. Blocking access to these clock instructions could hinder such attacks; however, legitimate users also depend on them for precise program measurements. Additionally, even if certain clock instructions are restricted, attackers could exploit alternative low-level timing mechanisms, such as timer interrupts [64]. Adding noise to these timers to obscure time differences has also been proposed as mitigation, as seen in prior work [65]. However, this approach incurs overhead, and recent studies [66] suggest that synthetic timers may still enable attackers to detect timing differences.

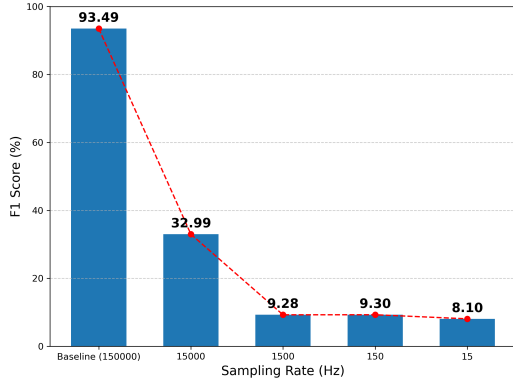


Figure 10: Application fingerprint attack results with limited frequency of *syncfs* calls.

**Detecting abnormal *syncfs* usage.** Our attack relies on continuous probing of *syncfs* timing delays, and a potential defense could involve monitoring for abnormal *syncfs* query patterns, such as using a daemon process to track suspicious *syncfs* activity. Previous research [67], [68] has explored malicious application detection by monitoring API call sequences and return values.

**Supporting isolation in I/O buffers.** Without changing the functionality of *syncfs*, we can redesign the write-back mechanism with minor changes. In our side channel attacks (§ 5.1 and § 5.2), we leak the write pattern of temporary files. These files do not need to be flushed to the disk since they should only be kept during the session. Therefore, a lightweight design is adding a tag for *open* that prevents the dirty pages of this file from being flushed by *syncfs*. We leave this as future work.

## 8. Related Work

**OS-level covert and side channel attacks.** The OS is designed to ensure isolation between multiple users or processes. However, researchers have demonstrated that side-channel leakages can compromise this isolation, exposing sensitive information like passwords and keystrokes. On Linux, Zhang and Wang [69] first demonstrated side-channel attacks via *procfs*, enabling the eavesdropping of users’ keystrokes. Qian et al. [70] then leveraged error packet counters in `/proc/net/` to execute off-path TCP session hijacking. Recently, Shen et al. [71] exploited mutual exclusion and synchronization mechanisms (MES) to establish covert channels for data transmission. On Android, Diao et al. [17] identified critical information leakage in Android’s interrupt handling mechanism. Similarly, on iOS, Zhang et al. [15] were the first to uncover OS-level side-channel vulnerabilities in iOS, exposing attack vectors such as memory and network usage APIs. Our work uncovers a novel vector of OS-level leakage, focusing specifically on file system synchronization calls within shared file systems.

**I/O-related attacks.** Our attacks fall into the category of I/O-related attacks. Prior research has demonstrated that

contention leakages on I/O can be exploited to establish covert and side channels. On one hand, timing leakages from contention have been shown on physical I/O components in modern computers, such as PCIe, CPU ring bus, and NVLink. For example, Tan et al. [9] introduced PCIe congestion side-channel attacks across GPUs, Network Interface Cards (NICs), and Solid-State Drives (SSDs). Similarly, Mert Side et al. [72] introduce a novel side channel vulnerability exploiting contention on the host-GPU PCIe bus, a critical interface in modern GPUs used in both traditional and cloud computing. Paccagnella et al. [73] propose the first microarchitectural side channel attacks leveraging contention on the CPU ring interconnect. Similar contention-based attacks have also been executed on other hardware architectures, such as CPU Mesh [74]. Recently, Zhang et al. [10] reveal vulnerabilities in NVLink interconnects, demonstrating a covert channel across GPUs and an application fingerprinting side channel attack using congestion-based timing leakages.

On the other hand, software I/O has also been investigated for contention-based leakages. Gruss et al. [75] introduced a software side-channel attack on the OS page cache, allowing unprivileged monitoring of memory access patterns. More recently, Jiang et al. [20] presented Sync+Sync, a timing-based covert channel leveraging contention in *fsync* calls on shared persistent storage. Similarly, Chen et al. [19] proposed a set of software cache write covert channels that exploit file system synchronization primitives.

Both of these works depend on contention from concurrent *fsync* API invocations and are limited to forming covert channels. Since most applications do not use the *fsync* API, this significantly restricts their potential for effective side-channel attacks. In contrast, our work exploits delay patterns in *syncfs*, a fundamentally different approach to contention-based leakages. Our method does not require the victim application to execute any I/O system calls, enabling us to implement both robust covert channels and high-resolution side channel attacks.

**Cross-container attacks.** Multi-tenancy is the feature of cloud computing that allows computation instances from different tenants to run on the same physical server. However, a series of work has demonstrated the cross-container attack on the cloud. Ristenpart et al. [76] is the first work on co-residence detection on the commercial cloud server. Gao et al. [77] identify information leakage channels in multi-tenancy container clouds caused by incomplete Linux kernel isolation mechanisms. Recently, Zhao et al. [78] conducted co-location attacks in public Function-as-a-Service (FaaS) environments, focusing on Google Cloud Run. Later, they successfully an end-to-end LLC Prime+Probe side-channel attack on Google Cloud Run [79].

## 9. Concluding Remarks

This work identified vulnerabilities in the *syncfs* system call that expose timing-based leakage vectors, compromising logical isolation. By exploiting these weaknesses,

we demonstrated high-bandwidth covert channels. Additionally, we developed three side-channel attacks for fingerprinting websites, videos, and applications. Furthermore, we explored cross-container attacks that breach isolation in containerized environments. Our findings highlight the need for improved defenses, such as redesigning *syncfs* and enhancing I/O buffer isolation. These measures are crucial to mitigating the identified risks while maintaining system functionality. Our attacks demonstrate that *syncfs*-based vulnerabilities pose a significant threat to system security.

## References

- [1] F. Rauscher, A. Kogler, J. Juffinger, and D. Gruss, "Idleleak: Exploiting idle state side effects for information leakage," in *Network and Distributed System Security (NDSS) Symposium 2024*, 2024.
- [2] D. Wang, Z. Qian, N. Abu-Ghazaleh, and S. V. Krishnamurthy, "Papp: Prefetcher-aware prime and probe side-channel attack," in *Proceedings of the 56th Annual Design Automation Conference 2019*, 2019, pp. 1–6.
- [3] F. Liu, Y. Yarom, Q. Ge, G. Heiser, and R. B. Lee, "Last-level cache side-channel attacks are practical," in *2015 IEEE symposium on security and privacy*. IEEE, 2015, pp. 605–622.
- [4] C. Slocum, Y. Zhang, N. Abu-Ghazaleh, and J. Chen, "Going through the motions: {AR/VR} keylogging from user head motions," in *32nd USENIX Security Symposium (USENIX Security 23)*, 2023, pp. 159–174.
- [5] R. Templeman, Z. Rahman, D. Crandall, and A. Kapadia, "Placeraider: Virtual theft in physical spaces with smartphones," *arXiv preprint arXiv:1209.5982*, 2012.
- [6] C. Slocum, Y. Zhang, E. Shayegani, P. Zaree, N. Abu-Ghazaleh, and J. Chen, "That doesn't go there: Attacks on shared state in {Multi-User} augmented reality applications," in *33rd USENIX Security Symposium (USENIX Security 24)*, 2024, pp. 2761–2778.
- [7] P. Pessl, D. Gruss, C. Maurice, M. Schwarz, and S. Mangard, "{DRAMA}: Exploiting {DRAM} addressing for {Cross-CPU} attacks," in *25th USENIX security symposium (USENIX security 16)*, 2016, pp. 565–581.
- [8] V. van der Veen and B. Gras, "Dramaqueen: Revisiting side channels in dram," 2023.
- [9] M. Tan, J. Wan, Z. Zhou, and Z. Li, "Invisible probe: Timing attacks with pcie congestion side-channel," in *2021 IEEE Symposium on Security and Privacy (SP)*. IEEE, 2021, pp. 322–338.
- [10] Y. Zhang, R. Nazaraliyev, S. B. Dutta, N. Abu-Ghazaleh, A. Marquez, and K. Barker, "Beyond the bridge: Contention-based covert and side channel attacks on multi-gpu interconnect," *arXiv preprint arXiv:2404.03877*, 2024.
- [11] H. Naghibijouybari, A. Neupane, Z. Qian, and N. Abu-Ghazaleh, "Rendered insecure: Gpu side channel attacks are practical," in *Proceedings of the 2018 ACM SIGSAC conference on computer and communications security*, 2018, pp. 2139–2153.
- [12] J. Wei, Y. Zhang, Z. Zhou, Z. Li, and M. A. Al Faruque, "Leaky dnn: Stealing deep-learning model secret with gpu context-switching side-channel," in *2020 50th Annual IEEE/IFIP International Conference on Dependable Systems and Networks (DSN)*. IEEE, 2020, pp. 125–137.
- [13] Y. Zhang, *Stealing Deep Learning Model Secret through Remote FPGA Side-channel Analysis*. University of California, Irvine, 2021.
- [14] Y. Zhang, R. Yasaei, H. Chen, Z. Li, and M. A. Al Faruque, "Stealing neural network structure through remote fpga side-channel analysis," *IEEE Transactions on Information Forensics and Security*, vol. 16, pp. 4377–4388, 2021.
- [15] X. Zhang, X. Wang, X. Bai, Y. Zhang, and X. Wang, "Os-level side channels without procs: Exploring cross-app information leakage on ios," in *Proceedings of the Symposium on Network and Distributed System Security*, 2018.
- [16] Z. Wang, J. Guan, X. Wang, W. Wang, L. Xing, and F. Alharbi, "The danger of minimum exposures: Understanding cross-app information leaks on ios through multi-side-channel learning," in *Proceedings of the 2023 ACM SIGSAC Conference on Computer and Communications Security*, 2023, pp. 281–295.
- [17] W. Diao, X. Liu, Z. Li, and K. Zhang, "No pardon for the interruption: New inference attacks on android through interrupt timing analysis," in *2016 IEEE Symposium on Security and Privacy (SP)*. IEEE, 2016, pp. 414–432.
- [18] Y. Zhang, C. Slocum, J. Chen, and N. Abu-Ghazaleh, "It's all in your head (set): Side-channel attacks on {AR/VR} systems," in *32nd USENIX Security Symposium (USENIX Security 23)*, 2023, pp. 3979–3996.
- [19] C. Chen, J. Cui, G. Qu, and J. Zhang, "Sync+ sync: Software cache write covert channels exploiting memory-disk synchronization," *arXiv preprint arXiv:2312.11501*, 2023.
- [20] Q. Jiang and C. Wang, "{Sync+ Sync}: A covert channel built on fsync with storage," in *33rd USENIX Security Symposium (USENIX Security 24)*, 2024, pp. 3349–3366.
- [21] R. H. Arpaci-Dusseau and A. C. Arpaci-Dusseau, "Operating systems: Three easy pieces," 2018.
- [22] J. C. Mogul, "A better update policy," in *USENIX Summer*, vol. 94, 1994.
- [23] M. Seltzer, P. Chen, and J. Ousterhout, "Disk scheduling revisited," in *Proceedings of the winter 1990 USENIX technical conference*. Washington, DC, 1990, pp. 313–323.
- [24] C. Silvers, "{UBC}: An efficient unified {I/O} and memory caching subsystem for {NetBSD}," in *2000 USENIX Annual Technical Conference (USENIX ATC 00)*, 2000.
- [25] V. Chidambaram, T. S. Pillai, A. C. Arpaci-Dusseau, and R. H. Arpaci-Dusseau, "Optimistic crash consistency," in *Proceedings of the Twenty-Fourth ACM Symposium on Operating Systems Principles*, 2013, pp. 228–243.
- [26] V. Chidambaram, T. Sharma, A. C. Arpaci-Dusseau, and R. H. Arpaci-Dusseau, "Consistency without ordering," in *FAST*, vol. 12, 2012, pp. 101–116.
- [27] G. R. Ganger and Y. N. Patt, "Metadata update performance in file systems," in *OSDI*, vol. 94, 1994, p. 5.
- [28] R. Haggman, "Reimplementing the cedar file system using logging and group commit," in *Proceedings of the eleventh ACM Symposium on Operating systems principles*, 1987, pp. 155–162.
- [29] X. Gao, Z. Gu, Z. Li, H. Jamjoom, and C. Wang, "Houdini's escape: Breaking the resource rein of linux control groups," in *Proceedings of the 2019 ACM SIGSAC Conference on Computer and Communications Security*, 2019, pp. 1073–1086.
- [30] Z. Wang, K. Sun, S. Jajodia, and J. Jing, "Disk storage isolation and verification in cloud," in *2012 IEEE Global Communications Conference (GLOBECOM)*. IEEE, 2012, pp. 771–776.
- [31] A. N. Bessani, R. Mendes, T. Oliveira, N. F. Neves, M. Correia, M. Pasin, and P. Verissimo, "Sefs: A shared cloud-backed file system," in *USENIX Annual Technical Conference*. Philadelphia, USA, 2014, pp. 169–180.
- [32] M. Cao, S. Bhattacharya, and T. Ts'o, "Ext4: The next generation of ext2/3 filesystems," in *LSF*, 2007.
- [33] A. Sweeney, D. Doucette, W. Hu, C. Anderson, M. Nishimoto, and G. Peck, "Scalability in the xfs file system," in *USENIX Annual Technical Conference*, vol. 15, 1996.
- [34] O. Rodeh, J. Bacik, and C. Mason, "Btrfs: The linux b-tree filesystem," *ACM Transactions on Storage (TOS)*, vol. 9, no. 3, pp. 1–32, 2013.

- [35] D. Hitz, J. Lau, and M. A. Malcolm, "File system design for an nfs file server appliance." in *USENIX winter*, vol. 94, 1994, pp. 10–5555.
- [36] ARM, "CNTVCT\_EL0, Counter-timer Virtual Count register," <https://developer.arm.com/documentation/ddi0601/2021-12/AArch64-Registers/CNTVCT-EL0--Counter-timer-Virtual-Count-register>, 2024.
- [37] L. Torvalds, "Documentation for /proc/sys/vm/," <https://github.com/torvalds/linux/blob/master/Documentation/admin-guide/sysctl/vm.rst>, 2024.
- [38] J. Mario and J. Eder, "Low latency performance tuning for red hat enterprise linux 7," 2017.
- [39] F. P. Miller, A. F. Vandome, and J. McBrewster, "Levenshtein distance: Information theory, computer science, string (computer science), string metric, damerau? levenshtein distance, spell checker, hamming distance," 2009.
- [40] H. Barnes, *Pro Windows Subsystem for Linux (WSL)*. Springer, 2021.
- [41] Alexa, "Top 1M sites (2024)," <https://www.alexa.com/topsites>.
- [42] D. Griffin and J. Lim, "Signal estimation from modified short-time fourier transform," *IEEE Transactions on acoustics, speech, and signal processing*, vol. 32, no. 2, pp. 236–243, 1984.
- [43] J. Huang, B. Chen, B. Yao, and W. He, "Ecg arrhythmia classification using stft-based spectrogram and convolutional neural network," *IEEE access*, vol. 7, pp. 92 871–92 880, 2019.
- [44] S. Chikkerur, A. N. Cartwright, and V. Govindaraju, "Fingerprint enhancement using stft analysis," *Pattern recognition*, vol. 40, no. 1, pp. 198–211, 2007.
- [45] P. Virtanen, R. Gommers, T. E. Oliphant, M. Haberland, T. Reddy, D. Cournapeau, E. Burovski, P. Peterson, W. Weckesser, J. Bright *et al.*, "Scipy 1.0: fundamental algorithms for scientific computing in python," *Nature methods*, vol. 17, no. 3, pp. 261–272, 2020.
- [46] K. He, X. Zhang, S. Ren, and J. Sun, "Deep residual learning for image recognition," in *Proceedings of the IEEE conference on computer vision and pattern recognition*, 2016, pp. 770–778.
- [47] A. Paszke, S. Gross, F. Massa, A. Lerer, J. Bradbury, G. Chanan, T. Killeen, Z. Lin, N. Gimelshein, L. Antiga *et al.*, "Pytorch: An imperative style, high-performance deep learning library," *Advances in neural information processing systems*, vol. 32, 2019.
- [48] R. Kohavi, "A study of cross-validation and bootstrap for accuracy estimation and model selection," *Morgan Kaufman Publishing*, 1995.
- [49] E. Ferguson, A. Wilson, and H. Naghibijouybari, "Webgpu-spy: Finding fingerprints in the sandbox through gpu cache attacks," *arXiv preprint arXiv:2401.04349*, 2024.
- [50] S. Wu, J. Yu, M. Yang, and Y. Cao, "Rendering contention channel made practical in web browsers," in *31st USENIX Security Symposium (USENIX Security 22)*, 2022, pp. 3183–3199.
- [51] R. D. Singh and N. Aggarwal, "Video content authentication techniques: a comprehensive survey," *Multimedia Systems*, vol. 24, pp. 211–240, 2018.
- [52] J. Gu, J. Wang, Z. Yu, and K. Shen, "Walls have ears: Traffic-based side-channel attack in video streaming," in *IEEE INFOCOM 2018-IEEE conference on computer communications*. IEEE, 2018, pp. 1538–1546.
- [53] A. Garboan, M. Mitrea, and F. Preteux, "Camcorder recording robust video fingerprinting," in *2012 IEEE 16th International Symposium on Consumer Electronics*. IEEE, 2012, pp. 1–4.
- [54] P. Błaskiewicz, M. Klonowski, and P. Syga, "Droppix: Towards more realistic video fingerprinting," 2020.
- [55] S. Tomar, "Converting video formats with ffmpeg," *Linux journal*, vol. 2006, no. 146, p. 10, 2006.
- [56] H. Zhang and K. Scheibe, "Multi-platform distribution of video content: An analysis of video content cross-posted by youtubers on bilibili," in *International Conference on Human-Computer Interaction*. Springer, 2023, pp. 149–156.
- [57] Amazon, "Amazon elastic container service (amazon ecs)," [https://aws.amazon.com/pm/ecs/?nc1=h\\_ls](https://aws.amazon.com/pm/ecs/?nc1=h_ls), 2024.
- [58] Google, "Containers on compute engine," <https://cloud.google.com/compute/docs/containers>, 2024.
- [59] A. Rebello, Y. Patel, R. Alagappan, A. C. Arpaci-Dusseau, and R. H. Arpaci-Dusseau, "Can applications recover from fsync failures?" *ACM Transactions on Storage (TOS)*, vol. 17, no. 2, pp. 1–30, 2021.
- [60] R. Verma, A. A. Mendez, S. Park, S. S. Mannarswamy, T. P. Kelly, and C. B. Morrey III, "{Failure-Atomic} updates of application data in a linux file system," in *13th USENIX Conference on File and Storage Technologies (FAST 15)*, 2015, pp. 203–211.
- [61] Y. Bai, L. Wu, X. Wu, X. Li, X. Zhang, and B. Wang, "Puf-based encryption method for ic cards on-chip memories," *Electronics Letters*, vol. 52, no. 20, pp. 1671–1673, 2016.
- [62] Y. Bai and Z. Yan, "A novel key generation scheme using quaternary puf responses and wiretap polar coding," *IEEE Communications Letters*, vol. 25, no. 7, pp. 2142–2145, 2021.
- [63] M. Li, Y. Yang, G. Chen, M. Yan, and Y. Zhang, "Sok: Understanding design choices and pitfalls of trusted execution environments," in *Proceedings of the 19th ACM Asia Conference on Computer and Communications Security*, 2024, pp. 1600–1616.
- [64] M. Schwarz, M. Lipp, D. Gruss, S. Weiser, C. L. N. Maurice, R. Spreitzer, and S. Mangard, "Keydrown: Eliminating software-based keystroke timing side-channel attacks," in *Network and Distributed System Security Symposium 2018*, 2018, p. 15.
- [65] J. Zhang, C. Chen, J. Cui, and K. Li, "Timing side-channel attacks and countermeasures in cpu microarchitectures," *ACM Computing Surveys*, vol. 56, no. 7, pp. 1–40, 2024.
- [66] S. B. Dutta, H. Naghibijouybari, A. Gupta, N. Abu-Ghazaleh, A. Marquez, and K. Barker, "Spy in the gpu-box: Covert and side channel attacks on multi-gpu systems," in *Proceedings of the 50th Annual International Symposium on Computer Architecture*, 2023, pp. 1–13.
- [67] M. Alazab, M. Alazab, A. Shalaginov, A. Mesleh, and A. Awajan, "Intelligent mobile malware detection using permission requests and api calls," *Future Generation Computer Systems*, vol. 107, pp. 509–521, 2020.
- [68] Z. Salehi, A. Sami, and M. Ghiasi, "Maar: Robust features to detect malicious activity based on api calls, their arguments and return values," *Engineering Applications of Artificial Intelligence*, vol. 59, pp. 93–102, 2017.
- [69] K. Zhang and X. Wang, "Peeping tom in the neighborhood: Keystroke eavesdropping on multi-user systems," in *USENIX Security Symposium*, vol. 20, 2009, p. 23.
- [70] Z. Qian, Z. M. Mao, and Y. Xie, "Collaborative tcp sequence number inference attack: how to crack sequence number under a second," in *Proceedings of the 2012 ACM conference on Computer and communications security*, 2012, pp. 593–604.
- [71] C. Shen, J. Zhang, and G. Qu, "Mes-attacks: Software-controlled covert channels based on mutual exclusion and synchronization," in *2023 60th ACM/IEEE Design Automation Conference (DAC)*. IEEE, 2023, pp. 1–6.
- [72] M. Side, F. Yao, and Z. Zhang, "Lockeddown: Exploiting contention on host-gpu pci bus for fun and profit," in *2022 IEEE 7th European Symposium on Security and Privacy (EuroS&P)*. IEEE, 2022, pp. 270–285.
- [73] R. Paccagnella, L. Luo, and C. W. Fletcher, "Lord of the ring (s): Side channel attacks on the {CPU}{On-Chip} ring interconnect are practical," in *30th USENIX Security Symposium (USENIX Security 21)*, 2021, pp. 645–662.
- [74] J. Wan, Y. Bi, Z. Zhou, and Z. Li, "Meshup: Stateless cache side-channel attack on cpu mesh," in *2022 IEEE Symposium on Security and Privacy (SP)*. IEEE, 2022, pp. 1506–1524.

- [75] D. Gruss, E. Kraft, T. Tiwari, M. Schwarz, A. Trachtenberg, J. Hennessey, A. Ionescu, and A. Fogh, "Page cache attacks," in *Proceedings of the 2019 ACM SIGSAC Conference on Computer and Communications Security*, 2019, pp. 167–180.
- [76] T. Ristenpart, E. Tromer, H. Shacham, and S. Savage, "Hey, you, get off of my cloud: exploring information leakage in third-party compute clouds," in *Proceedings of the 16th ACM conference on Computer and communications security*, 2009, pp. 199–212.
- [77] X. Gao, B. Steenkamer, Z. Gu, M. Kayaalp, D. Pendarakis, and H. Wang, "A study on the security implications of information leakages in container clouds," *IEEE Transactions on Dependable and Secure Computing*, vol. 18, no. 1, pp. 174–191, 2018.
- [78] Z. N. Zhao, A. Morrison, C. W. Fletcher, and J. Torrellas, "Last-level cache side-channel attacks are feasible in the modern public cloud," in *Proceedings of the 29th ACM International Conference on Architectural Support for Programming Languages and Operating Systems, Volume 2*, 2024, pp. 582–600.
- [79] —, "Everywhere all at once: Co-location attacks on public cloud faas," in *Proceedings of the 29th ACM International Conference on Architectural Support for Programming Languages and Operating Systems, Volume 1*, 2024, pp. 133–149.